An energy-based prognostic framework to predict evolution of damage in composite materials

16

M. Chiachío [1], J. Chiachío [1], A. Saxena [2], K. Goebel [3]
[1]University of Granada, Campus de Fuentenueva, Granada, Spain; [2]General Electric Global Research, San Ramon, United States; [3]NASA Ames Research Center, Intelligent Systems Division, Moffett Field, United States

16.1 Introduction

Composite materials are high-performance engineering materials increasingly used by the aerospace industry in part because of their high strength-to-weight ratios. Fatigue damage represents one of the most important sources of concern for in-service performance, which has led to growing research interest in industry and academia. Influenced by a long-standing understanding of the principles of metal fatigue, the initial treatment for fatigue behavior in composites was similar to metallic structures [1], and as a consequence, numerous models were formulated as extensions of metal fatigue theories [2]. However, unlike metals, fatigue damage in composites comprises multiple simultaneous internal fracture mechanisms such as matrix microcracks, delamination, fiber breakage, etc., that ultimately lead to significant changes in the macroscale mechanical properties of the material over its lifespan [3,4]. This multivariate damage process leads to uncertainty in assessment of current and future material properties. This stems in part from the material heterogeneity and an incomplete knowledge about the physics behind the evolution and interaction of damage mechanisms. Fatigue damage predictions using deterministic models in absence of any ground truth information about the current degradation state are not expected to provide much accurate information about the state of health of the material.

However, real-time measurements of the structural performance are now possible through state-of-the-art structural health monitoring (SHM) techniques, and a large amount of response data can be readily acquired and further analyzed to assess various health-related properties of structures. Therefore, a more suitable approach for fatigue damage prediction is through the use of monitored response of the structure to update a given damage model so as to make more accurate predictions that also account for uncertainty. Development of such SHM-based damage prognostics approach is the core objective of this chapter.

Structural Health Monitoring (SHM) in Aerospace Structures. http://dx.doi.org/10.1016/B978-0-08-100148-6.00016-0

Damage prognostics is concerned with predicting the future health state of engineering systems or components given current degree of wear or damage, and, based on that, estimating the remaining time beyond which the system is expected not to perform its intended function within desired specifications. This estimated remaining time is referred to as the remaining useful life (RUL). Algorithms that estimate RUL make use of the information coming from damage models and SHM data to propagate the estimated health state into the future and as output provide an estimate of time where the component no longer meets its desired functionality.

Over the last years the topic of fatigue damage prognostics has slowly gained interest [5e9] although the focus has been predominantly on fatigue crack growth in metals. In this chapter a model-based prognostics framework is proposed to predict a sequence of damage states of composite laminates subjected to fatigue loading. Damage states as well as model parameters of the underlying damage model are sequentially updated and predicted based on available SHM data. The proposed methodology is implemented and demonstrated using data for microcrack density and stiffness reduction in carbon fiber reinforced plastic (CFRP) cross-ply laminates from run-to-failure tensione tension fatigue experiments.

16.2 Fundamentals

Prognostics aims at determining the end of life (EOL) and RUL of components or systems given the information about the current degree of wear or damage, the component's load history, and the anticipated future load and environmental conditions. In prognostics the EOL is defined as the limiting time when an asset is expected to depart from the serviceability conditions. RUL is the period of remaining time from the current time (or time of prediction) until estimated EOL.

Prognostics can be seen as a natural extension of SHM in the sense that the predictions of RUL and EOL are frequently updated using data from a sensing system. It is rather a sequential process of updatee predicte reassess where the user is not only concerned with detecting, isolating, and sizing a fault mode, but also with (1) predicting the remaining time before the failure occurs, and (2) quantifying the uncertainty in the prediction, that can be further used for risk assessment and rational decision-making. Henceforth, prognostics requires periodic SHM measurements to reassess and improve the quality of the predictions of EOL and RUL as time goes by. After a brief overview of prognostics solutions in aerospace structures the following sections briefly discuss various aspects involved in design of a prognostics health management (PHM) system.

16.2.1 PHM for aerospace structures

Aerospace structures are a class of lightweight structures used for aircrafts and spacecrafts which are normally subjected to cyclic loads. Preventing fatigue damage failure resulting from cyclic loads requires damage monitoring and inspection, and thus scheduled maintenance to be done over the vehicle's operational life, which notably increases the direct operating costs [10]. One of the major issues for aircraft operators, as well as for aircraft assemblers, is to reduce the direct operating costs without

compromising the safety. Within this scenario, damage prognostics emerges as a rational approach as it enables cost-effective risk-based maintenance schedules based on predictions of the RUL [11]. Future damage predictions can be obtained with quantified uncertainty and are based on knowledge about current damage state of the structure using SHM.

In the SHM literature, there are a growing number of articles dealing with prognostics solutions for aerospace structures. For example, a prognostics framework was presented in application to fatigue degradation of a composite wing from an unmanned aerial vehicle [12]. SHM data were obtained through in-flight tests as well as through on-ground inspections, and predictions were performed to obtain both local and component-level measures of damage. The Joint Strike Fighter Autonomic Logistics [13] is another example of application of the PHM sciences to the aircraft industry, where the prognostics architecture is conceived to be applied at the level of the entire vehicle (system level) through the integration of subsystem prognostics reasoners for different components: structures, engines, communication systems, etc. In the helicopter industry, damage prognostics has acquired considerable significance for health maintenance. A remarkable example of this category is the health and usage monitoring systems for main rotor and gearbox components on large rotorcrafts, which has been shown capable of considerably reducing the fatal hull loss [14], while increasing the rotor component life by about 15% [15].

The aforementioned examples represent just a few of the different prognostics approaches that are encountered in the literature on application to aerospace structures. However, although some of these prognostics approaches have successfully made the transition from research to practice, damage prognostics still requires more research efforts and further development, and needs to be justified by significant impact on safety and economy overall when applied to aerospace composite structures.

16.2.2 Design for prognostics

The design of a prognostics system is of paramount importance to ascertain that the prognostic solution meets expectations. For example, reduction of life cycle cost, safety improvement, or an optimization of uptime to better guarantee mission availability, are just few examples of goals to be accomplished by the prognostics solution. In a general sense the design process needs to be considered as part of a systems engineering process. Design process can be conceptually partitioned into three stages: analysis, concept, and synthesis, as Fig. 16.1 illustrates.

During the analysis phase, requirements for the overall system are established based on a set of predefined goals and the end use of prognostics [17]. Next the prognostics functionality is defined during the concept phase. In this phase, functional needs and constraints are determined to drive potential solutions to the system in presence of any faulty behavior. Key concepts at this phase are observability of fault modes and assessment of prediction performance, which are both further explained in Sections 16.2.2.1 and 16.2.2.2. Finally the functional needs are encapsulated in appropriate physics-based models that characterize the system fault propagation as well as the system final failure. During this phase, suitable algorithms are developed to efficiently predict the future faulty behavior of the system.

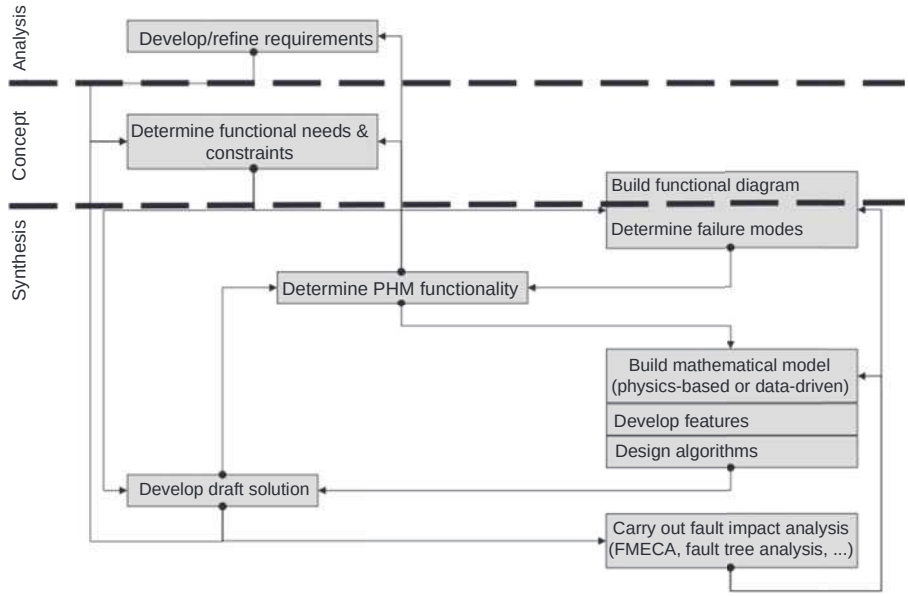

Figure 16.1 Schematic description for the design process of a PHM solution [16]. FMECA, failure mode, effects and criticality analysis.

The majority of this chapter is dedicated to delineating the models and algorithms one can use in the context of composite materials.

16.2.2.1 Observability of fault modes

Using suitable sensors that can interrogate the system health state and assess in real time any change in fault severity are of paramount importance. Because damage predictions are sequentially updated from periodical measurements, the higher the accuracy expected from prognostics, the better the quality required for the information obtained from the sensing system. However, this information comes at the expense of more targeted sensing and significant computational requirements. Complex systems subjected to a variety of fault modes (cracks, voids, delamination, corrosion, etc.) that often require dedicated sensors and sensor networks for detection as no one sensor type can typically provide sufficient information to cover all fault modes. The choice of the sensing method is typically guided by the feature or set of features to be monitored. For example, weight loss or power demand sensors onboard airspace systems results in a different sensor choice than for monitoring vibrations in buildings or corrosion in bridge structures [18].

Sensor locations are chosen such that the expected type of damage produces observable and statistically significant effects in features derived from the measurements at these locations, which is often determined through numerical simulations or physical tests. Low-level local response caused by damage (eg, cracks opening and closing) must be separated from large-amplitude global response, such as that caused by aerodynamic loads on aircrafts, by determining required sensitivity and dynamic range

through analysis or experimentation. There are several methods for optimal placement of sensors that consider maximum information quality (see for example Ref. [19]).

16.2.2.2 Prognostic performance metrics

Once a component or subsystem is being monitored using an appropriate sensor system the next requirement for an efficient prognostics framework resides in quantifying the prediction performance. Decisions based on poor and/or late predictions may increase the risk of system failure, whereas wrong predictions of failure (false positives) trigger unnecessary maintenance actions with unavoidable cost increase.

A detailed discussion about deriving prognostics requirements from top level system goals was proposed by Saxena et al. [20]. These requirements are generally specified in terms of prediction performance that prognostics must satisfy for a desired level of safety or cost benefit. A variety of prognostics performance evaluation metrics have been defined in the literature, like prediction horizon (PH), a e l accuracy measure, and relative accuracy measures [21,22]. As described by Saxena et al. [23] prognostics performance can be summarized by three main attributes, namely:

correctness, which is related to the prediction accuracy when compared with observed outcomes;

timeliness, which accounts for how fast an algorithm produces the output as compared to the rate of upcoming outcomes from the system; and

confidence, which deals with the uncertainty in a prognostics output, typically from a prognostics algorithm.

Among the metrics proposed by Saxena et al. [21,22] the PH and the a e l accuracy measures are widely used in prognostics and also adopted for this work. The PH serves to determine the maximum early warning capability that a prediction algorithm can provide with a user-defined confidence level denoted by a. Typically, a graphical representation using a straight line with negative slope serves to illustrate the "true RUL," that decreases linearly as time progresses. The predicted probability density functions (PDFs) of RUL are plotted against time of prediction using error bars (eg, by 5e 95% error bars) as Fig. 16.2 (left panel) shows.

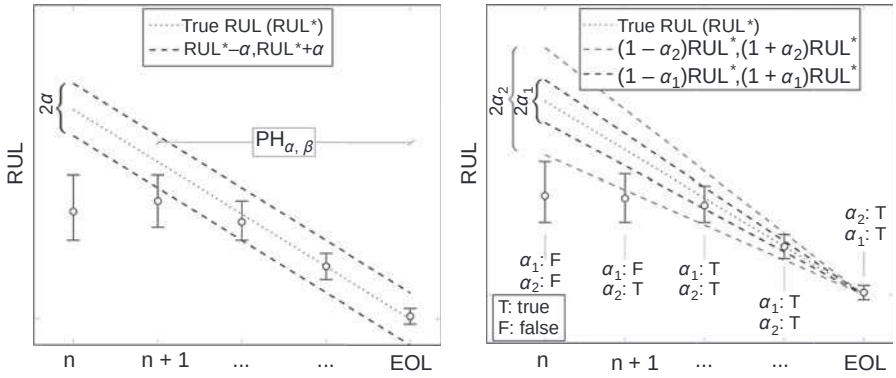

Figure 16.2 Illustrations of (left) PH and (right) a! l prognostics metrics.

Ideally the median of the RUL predictions should stay on the dotted line (RUL*) that represents the true RUL, or, at least, stay within the accuracy regions specified by a. By means of this representation the PH can be directly determined as shown in Fig. 16.2 (left). The PH metric can be further parameterized by a parameter b (thus denoted by $PH_{a,b}$) that specifies the minimum acceptable probability of overlap between the predicted RUL and the a accuracy bands delimited by the dashed lines in Fig. 16.2 (left). Both a and b are scaling parameters for the prognostics which should be fixed considering the application scenario.

For the ae l accuracy metric a straight line with a negative slope is also used to represent the true RUL. Predicted PDFs of RUL are plotted against time of prediction (which is termed as l in the original paper by Saxena et al. [22]) using error bars. As in Fig. 16.2 (left), accurate predictions should lie on this line as long as they are sequentially updated with SHM data. In this case the accuracy region is determined by parameter a, which represents a percentage of the true RUL so that it denotes the notion that accuracy of prediction becomes more critical as EOL approaches. See Fig. 16.2 (right) for illustration. In this case, two confidence regions are employed by adopting $0 < a_1 < a_2 < 1$, so that each predicted RUL can be validated depending on whether or not it belongs to any of the a_1 or a_2 regions.

16.2.3 Fundamentals of model-based prognostics

A complete and rigorous prognostics solution hinges on the availability of several elements, that include a model for system health evolution, a quantifiable criterion for what constitutes failure, and a method to deal with underlying uncertainties. Typically, it is accomplished in three steps that are addressed in this section: (1) current state estimation, (2) future state prediction, and (3) RUL estimation. In order to carry out the steps above, a generic time-dependent, statee space modeling framework is presented first.

16.2.3.1 Statee space system modeling

Let us consider a generic component or subsystem whose health state is expected to evolve as follows:

$$x_n ¼ g(x_{n-1}; u_n; q) v_n \quad [16.1]$$

where $g(x_{n-1}; u_n; q) : R^{n_x} \& R^{n_u} \& R^{n_q} / R^{n_x}$ is a possibly nonlinear function of the system state $x_n ¸ R^{n_x}$ that may depend on a set of n_q (uncertain) model parameters $q ¸ Q 3 R^{n_q}$, along with a set $u_n ¸ R^{n_u}$ of input parameters to the system (loadings, environmental conditions, operating conditions, etc.). The term $v_n ¸ R^{n_x}$ refers to the model error, which represents the difference between the actual system state x_n and the state predicted by the hypothesized model $g(x_{n-1}, u_n, q)$.

In addition, it is assumed that measurements of the system health state can be obtained during operation and that, at a certain time, n, the measured system state,

y_n, can be expressed as a function of the latent state, x_n, by means of the following measurement equation:

$$y_n = x_n + w_n \quad [16.2]$$

where w_n is the measurement error. It is also assumed that the error terms v_n and w_n from Eqs. [16.1] and [16.2] are random variables instead of deterministic fixed-valued variables, and that they are distributed following specified probability models. Based on these probability models the PDFs for the state transition equation and observation equation are prescribed. For example, when errors v_n and w_n are modeled as zero-mean Gaussian distributions, which is supported by the principle of maximum information entropy [24]. The state transition equation and the observation equation defined in Eqs. [16.1] and [16.2], respectively, can be expressed as Gaussian distributions as follows:

$$p(x_n|x_{n-1}; u_n; q) = (2\pi)^{-n_x/2}|S_{v_n}|^{-1/2}\exp\left(-\frac{1}{2}(x_n - \bar{x}_n)^T S_{v_n}^{-1}(x_n - \bar{x}_n)\right) \quad [16.3]$$

$$p(y_n|x_n; q) = (2\pi)^{-n_x/2}|S_{w_n}|^{-1/2}\exp\left(-\frac{1}{2}(y_n - x_n)^T S_{w_n}^{-1}(y_n - x_n)\right) \quad [16.4]$$

where $\bar{x}_n = g(x_{n-1}; u_n; q)$, and $S_{v_n} \in R^{n_x \times n_x}$ and $S_{w_n} \in R^{n_x \times n_x}$ are the covariance matrices of the model error and the measurement error, respectively. Eqs. [16.3] and [16.4] constitute the stochastic equations for the overall system response, and play a major role in the proposed model-based prognostics framework.

16.2.3.2 Sequential state estimation

Once the system has been mathematically described using the stochastic system equations given above the first step for prognostics is to recursively update the joint PDF of the system health state x_n along with model parameters q at every time n a new measurement is collected.

To this end, let us define an augmented state $z_n = (x_n; q) \in Z = R^{n_x} \times R^{n_q}$ representing the overall system response including model parameters $q \in Q$. Thus, given a sequence of measurements up to time n, namely $y_{0:n} = \{y_0, y_1, \ldots, y_{n-1}, y_n\}$, the goal is to estimate the posterior probability of the up-to-date sequence of states $z_{0:n} = \{z_0, z_1, \ldots, z_{n-1}, z_n\}$, expressed by the conditional PDF $p(z_{0:n}|y_{0:n})$. This is accomplished by Bayes' theorem as follows:

$$p(z_{0:n}|y_{0:n}) = \frac{p(y_n|z_n)p(z_{0:n}|y_{0:n-1})}{\int p(y_n|z_n)p(z_{0:n}|y_{0:n-1})dz_{0:n}} \quad [16.5]$$

$$\propto p(y_n|z_n)p(z_n|z_{n-1})p(z_{0:n-1}|y_{0:n-1})$$

last update

where

$$p(z_n|z_{n-1}) = p(x_n|x_{n-1}, q_n)\, p(q_n|q_{n-1}) \quad [16.6]$$

Eq: 16.3

$$p(y_n|z_n) = p(y_n|x_n, q_n) \quad [16.7]$$

Eq: 16.4

As observed in Eq. [16.3], model parameters q_n are assumed to evolve by some unknown random process that is independent of the system state, x_n. It should be noted that model parameters are essentially not dependent on time, and hence $p(q_n|q_{n-1})$ implies an "artificial" evolution given the nondynamic nature of q. A followed solution to obtain a model for $p(q_n|q_{n-1})$ is to add an independent random perturbation x_n to the set of updated parameters at time $n-1$ before evolving to the next predicted state at time n [25,26]; ie, $q_n = q_{n-1} + x_n$, whereby the PDF $p(q_n|q_{n-1})$ is prescribed. For example, if x_n is assumed to follow a zero-mean Gaussian, thus:

$$p(q_n|q_{n-1}) = N\left(q_{n-1}; S_{x_n}\right) \quad [16.8]$$

Observe that by this method, an additional source of uncertainty is artificially introduced to the model parameters leading to a loss of information about q (ie, larger spread bands) over time that ultimately influences the precision of the state estimation. To sequentially reduce this additional uncertainty, several methods have been proposed in the literature [26e 28], with the most popular being those that impose some kind of shrinkage over S_{x_n} as long as new data are collected [26]. An efficient method of this class has been proposed by Daigle and Goebel [29], which is adopted in this work by its simplicity and efficiency.

16.2.3.3 Sampling method for sequential state estimation

The sequential state estimation methodology presented above is analytically intractable except some especial cases using both linear models and Gaussian uncertainties. For the general case of nonlinear models and/or non-Gaussian uncertainties, sampling-based algorithms like particle filters (PFs) [30,31] have been shown to efficiently approximate the updating PDF $p(z_{0:n}|y_{0:n})$ by means of a set of N discrete particles $\left\{z_{0:n}^{(i)}\right\}_{i=1}^{N}$ with associated weights $\left\{u_n^{(i)}\right\}_{i=1}^{N}$. By PF the required PDF is approximated as:

$$p(z_{0:n}|y_{0:n}) \approx \sum_{i=1}^{N} u_n^{(i)}\, \delta\left(z_{0:n} - z_{0:n}^{(i)}\right) \quad [16.9]$$

where d is the Dirac delta. In practice, it is not possible to obtain samples directly from $p(z_{0:n}|y_{0:n})$ as it is seldom known exactly, hence a common solution is to generate samples from an importance density PDF $q(z_{0:n}|y_{0:n})$ which is easier to simulate, leading to the sequential importance sampling (SIS) approach. To compensate for the difference between the importance density and the true posterior density the unnormalized weights are defined as follows:

$$\tilde{w}_n^{(i)} = \frac{p\left(z_{0:n}^{(i)}|y_{0:n}\right)}{q\left(z_{0:n}^{(i)}|y_{0:n}\right)} \tag{16.10}$$

where $u_n^{(i)} = \frac{\tilde{w}_n^{(i)}}{\sum_{i=1}^{N} \tilde{w}_n^{(i)}}$, $i = 1, \ldots, N$. There is a vast literature dealing with optimal selection strategies for the importance density PDF [30,32]; however, in most of the practical applications the importance density is conveniently chosen so that it admits a sample procedure by adopting $q(z_{0:n}|y_{0:n}) = q(z_{0:n}|y_{0:n-1})$, hence it can be factorized in a form similar to that of the updating PDF, ie, $q(z_{0:n}|y_{0:n-1}) = q(z_n|z_{n-1})q(z_{0:n-1}|y_{0:n-1})$. Thus, by substituting Eq. [16.5] into Eq. [16.10], the unnormalized importance weight for the ith particle at time n can be rewritten as:

$$\tilde{w}_n^{(i)} \propto \underbrace{\frac{p\left(z_{0:n}^{(i)}|y_{0:n-1}\right)}{q\left(z_{0:n-1}^{(i)}|y_{0:n-1}\right)}}_{u_{n-1}^{(i)}} \frac{p\left(z_n^{(i)}|z_{n-1}^{(i)}\right) p\left(y_n|z_n^{(i)}\right)}{q\left(z_n^{(i)}|z_{n-1}^{(i)}\right)} \tag{16.11}$$

In addition the PDF $q(z_n|z_{n-1})$ in Eq. [16.11] is typically chosen to coincide with the state transition equation $p(z_n|z_{n-1})$ [25] defined in Eq. [16.6], as it is straightforward to evaluate. In this case, Eq. [16.11] simplifies to:

$$\tilde{w}_n^{(i)} \propto u_{n-1}^{(i)} p\left(y_n|z_n^{(i)}\right) \tag{16.12}$$

and the resulting algorithm is commonly known as a "bootstrap filter," after the celebrated paper by Gordon et al. [25]. A pseudocode implementation for the PF is given as Algorithm 2 in Section 16.4, in the context of the prognostics example in composites. Algorithm 2 includes a systematic resampling step [30] to limit the well-known degeneracy problem.[1]

[1] During resampling, particles are either dropped or reproduced that may result in a loss of diversity of the particle paths [30]. If necessary, a control step of degeneracy by quantifying the effective sample size (ESS) may be incorporated before the resampling.

16.2.3.4 Future state prediction

Having estimated the current health state of the system at time n by means of the methodology explained above the next step for prognostics is to predict the future states of the system ‘-steps forward in time in absence of new observations, ie, $p(z_{n+\ell}|y_{0:n})$, with ‘ > 1. This distribution can be obtained by the total probability theorem as:

$$p(z_{n+\ell}|y_{0:n}) = \int p(z_{n+\ell}|z_{n:n+\ell-1}) p(z_{n:n+\ell-1}|y_{0:n}) dz_{n:n+\ell-1} = \int \left[\prod_{t=n+1}^{n+\ell} p(z_t|z_{t-1}) \right] p(z_n|y_{0:n}) dz_{n:n+\ell-1} \quad [16.13]$$

where it uses the fact that $p(z_{n+\ell}|z_{n:n+\ell-1}) = p(z_{n+\ell}|z_{n+\ell-1})$, ‘ > 1, as Eq. [16.1] defines a Markov model of order one and also by the assumption that the observations are conditionally independent given the states. Replacing $p(z_n|y_{0:n})$ in the last equation by its PF approximation, an approximation to the PDF $p(z_{n+\ell}|y_{0:n})$ is obtained as follows:

$$p(z_{n+\ell}|y_{0:n}) \approx \int \left[\prod_{t=n+1}^{n+\ell} p(z_t|z_{t-1}) \right] \sum_{i=1}^{N} w_n^{(i)} \delta\left(z_{0:n} - z_{0:n}^{(i)}\right) dz_{n:n+\ell-1}$$
$$= \sum_{i=1}^{N} w_n^{(i)} \int p\left(z_{n+1}|z_n^{(i)}\right) \prod_{t=n+2}^{n+\ell} p(z_t|z_{t-1}) dz_{n+1:n+\ell-1} \quad [16.14]$$

Observe that Eq. [16.14] corresponds to a weighted sum of integrals that can be readily simulated by drawing one conditional sample sequence $z_{n+1:n+\ell}^{(i)} = \left\{ z_{n+1}^{(i)}, z_{n+2}^{(i)}, \ldots, z_{n+\ell}^{(i)} \right\}$ from each of the N multidimensional integrals in Eq. [16.14] using recursively the state transition equation (recall Eq. [16.6]): ie, first sample $z_{n+1}^{(i)}$ using the aforementioned one-step transition equation conditional on the initial state, z_n, ie, $z_{n+1}^{(i)} \sim p\left(z_{n+1}|z_n^{(i)}\right)$; then sample the succeeding state conditional on the previous sample, ie, $z_{n+2}^{(i)} \sim p\left(z_{n+2}|z_{n+1}^{(i)}\right)$; finally, repeat the same process until the target time n þ ‘ is reached.

16.2.3.5 RUL prediction

To obtain the EOL and RUL based on the predicted future state of the system given by $p(z_{n+\ell}|y_{0:n})$ the definition of a useful domain for the predicted states is first required. Let $U \subset Z$ be the nonempty subset of authorized states of the system, whereas the complementary subset, $\bar{U} = Z \setminus U$ corresponds to the subset of states where system failure occurs. Without loss of generality the useful domain can be delimited by means of a

set of n_c constrains $\{c_1; c_2; \ldots; c_{n_c}\}$, where each one represents a function that maps a given point z in the joint state-parameter space to the Boolean domain {0,1}, ie, $c_j: Z \rightarrow \{0,1\}$, such that $c_j(z) = 0 \Leftrightarrow z \in \bar{U}; j = 1; \ldots; n_c$. In other words, $z \in \bar{U}$ when any of the constraints are violated.

Using the PF approach defined above the EOL predicted at time n can be obtained for the ith particle trajectory as the earliest time $t' \geq n$ when the event $z_t^{(i)} \in \bar{U}$ occurs. In mathematical terms:

$$EOL_n^{(i)} = \inf\left\{t \in \mathbb{N} : t' \geq n \wedge I_{\bar{U}}\left(z_t^{(i)}\right) = 1\right\} \quad [16.15]$$

where $I_{\bar{U}}(\#)$ is an indicator function for the region $\bar{U}$ that assigns a value of 1 when $z \in \bar{U}$ and 0 otherwise. The RUL predicted at time n for the ith particle can be obtained using $EOL_n^{(i)}$ as:

$$RUL_n^{(i)} = EOL_n^{(i)} - n \quad [16.16]$$

Fig. 16.3 provides a schematic illustration to exemplify the trajectory of the ith particle of a z-state of dimension two (for ease of representation) along with the indication of $EOL_n^{(i)}$ and $RUL_n^{(i)}$.

By repeating the process for each particle $i = 1, \ldots, N$, an approximation to the PDF of EOL at time n can be obtained as:

$$p(EOL_n | y_{0:n}) \approx \sum_{i=1}^{N} u_n^{(i)} \delta\left(EOL_n - EOL_n^{(i)}\right) \quad [16.17]$$

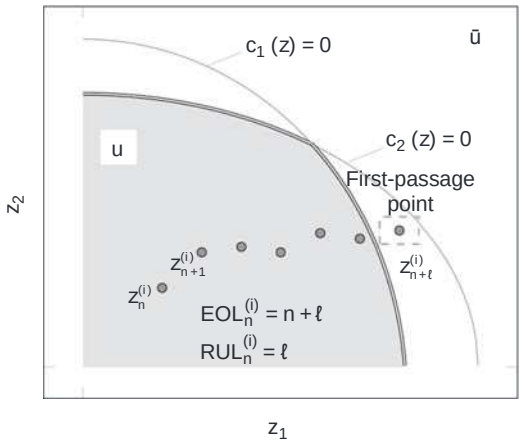

Figure 16.3 Two-dimensional illustration of the ith particle trajectory to EOL. A sequence of samples in the Z-space, ie, $z_n^{(i)}; z_{n+1}^{(i)}; \ldots; z_{n+\ell}^{(i)}$ are represented using solids disks. Two constraint functions $\{c_1(z), c_2(z)\}$ are represented.

Correspondingly the PDF of RUL_n can be approximated as:

$$p(RUL_n|y_{0:n}) \approx \sum_{i=1}^{N} u_n^{(i)} \delta\left(RUL_n - RUL_n^{(i)}\right) \quad [16.18]$$

An algorithmic description of the prognostics procedure is provided as Algorithm 1.

Algorithm 1: PF-based prognostics algorithm.

1. inputs: $\left\{z_n^{(i)} = \left(x_n^{(i)}, q_n^{(i)}\right), u_n^{(i)}\right\}_{i=1}^{N}$, updated particles at time n. Use eg, Algorithm 2 given further below.
2. Define $U \subseteq Z$, {[useful domain}]
3. for i = 1 to N do
4. $t \leftarrow n$
5. $z_t^{(i)} \leftarrow z_n^{(i)}$
6. Evaluate $EOL_n^{(i)}\left(z_t^{(i)}\right)$
7. while $I_U\left(z_t^{(i)}\right) = 0$ do
8. Predict u_t
9. Sample $q_{t+1}^{(i)} \sim p\left(q_{t+1}|q_t^{(i)}\right)$
   $x_{t+1}^{(i)} \sim p\left(x_{t+1}|x_t^{(i)}, q_{t+1}^{(i)}, u_t\right)$
10. $t \leftarrow t+1$
11. $z_t = \left(x_t^{(i)}, q_t^{(i)}\right) \rightarrow z_{t+1} = \left(x_{t+1}^{(i)}, q_{t+1}^{(i)}\right)$
12. end while
13. $EOL_n^{(i)} \leftarrow t$
    $RUL_n^{(i)} = EOL_n^{(i)} - n$
14. end for

16.3 Damage prognostics in composite materials

Anticipating the occurrence and growth of damage states in the material in future is of crucial importance for determining the remaining time for which the structure is desired to perform per specifications. To this end, first the relevant damage modes are identified and suitable models for damage evolution are developed. This enables predictions of future damage states that are sequentially updated using the information from sensors. In this section a physics-based modeling framework is presented for damage evolution in composites and a discussion about selecting damage thresholds is provided. Additionally, the connection between proposed damage models and the

model-based prognostics framework, as discussed in Section 16.2.3, is examined at the end of this section.

16.3.1 Damage propagation model

The progression of fatigue damage in composites involves a progressive or sudden change of the macroscale mechanical properties, such as stiffness or strength, as a consequence of different fracture modes that evolve at the microscale level during the lifespan of the structure [4]. Through decades of investigation, numerous fatigue models have been proposed in the literature [2]. A vast majority of them are deterministic semiempirical formulations often customized for specific material configuration under specific testing/loading conditions. The publications that have incorporated uncertainty in fatigue modeling have primarily used Markov chain models and other stochastic models for fatigue damage evolution [33]. These approaches suffer from the fact that models used therein often lack physical meaning and are purely empirical in nature. One of the most widely used models for metallic structures is Paris' law [34] that relates a crack's length growth rate to the range of applied stress intensity factor primarily because it is better associated with the physics of the damage growth process. However, in contrast to metals, composites under fatigue loading exhibit growing density of multiple interlaminar and intralaminar microcracks [35] instead of a single crack growth. Due to its simple formulation and associated physical interpretation of damage, Paris' law is still a preferred choice for composite materials and the modified Paris' law [36] emerged as the best suited model for fatigue in composites. A description of the model is given as follows:

$$\frac{dr}{dn} = A(\Delta G)^{\alpha} \qquad [16.19]$$

where A and α are fitting parameters and r is the microcrack's density that increases as fatigue cycles, n, evolve. The term ΔG is the energy release rate (ERR), and represents the energy released due to the formation of a new crack between two existing cracks at a specific stress amplitude: $\Delta G = G_{|S_{max}} - G_{|S_{min}}$, which can be calculated as [37]:

$$\Delta G = \frac{\Delta s_x^2 h}{2 r t_{90}} \left(\frac{1}{E_x^{(}(2r)} - \frac{1}{E_x^{(}(r)} \right) \qquad [16.20]$$

In the last equation, Δs_x is the increment in applied axial tension, and h and t_{90} are the laminate and 90 degree sublaminate half-thickness, respectively. The term $E_x^{(}(r)$, as a function of r, is the effective laminate Young's modulus due to the current damage state which can be calculated using a suitable damage mechanics model such as those presented in Section 16.3.2. It follows that closed-form solutions for $r = r(n)$ are rarely available as ΔG involves complex expressions for damage mechanics models. To overcome this drawback the resulting differential equation can be solved by

approximating the derivative using the "unit-time" finite difference approach, assuming that damage evolves cycle-to-cycle as:

$$r_n = r_{n-1} + \Delta G(r_{n-1})^{\alpha} \quad [16.21]$$

16.3.2 Micro- to macroscale damage model

To accurately represent the relation $E_x^{(} = E_x^{(}(r)$ in Eq. [16.20], several families of damage mechanics models have been proposed in the literature [38]. These models are based on first principles of admissible ply stress fields in the presence of damage, and can be roughly classified into (1) analytical models, (2) semianalytical models, and (3) computational models. Among them, computational and semianalytical models have been shown to be promising, however, they are computationally prohibitive in a filtering-based prognostics approach as large amounts of model evaluations are required. Surrogate models may alleviate that problem by adopting data-driven techniques. A more detailed discussion of such techniques is beyond the scope of this chapter and the focus is instead on a set of analytical models. Depending on the level of assumptions adopted to model the stress field in the presence of damage, they can be classified (from simpler to more complex) into shear lag models [39], variational models [40], and crack opening displacement (COD)-based models [41]. Among them the shear lag models are simpler and have received significant attention in the literature [38]. The main modeling assumption in shear lag models is that, at the matrix crack locations, the axial load is transferred to uncracked plies by the axial shear stresses acting at the interfaces. These models are usually restricted to cross-ply laminates or $[f_{\frac{n_f}{2}}/90_{n_{90}}/f_{\frac{n_f}{2}}]$ layups, where $f_{\zeta}^{)} \in [90^{)}, 90^{)}]$ is the ply-angle of the outer sublaminates (see Fig. 16.4). However, it should be noted that the prognostics methodology presented in this chapter is not restricted to the above class of models and is applicable to any other suitable damage model class. In this work the classical shear lag model [39,42] is chosen to represent the relation between microcrack density (as the microscale damage variable), and relative stiffness decrease (as macroscale damage manifestation). The classical shear lag model provides reasonably accurate results and is shown to be less sensitive to the noise in data, as presented in a study [43]. From this standpoint, matrix microcracking is selected as dominant fracture mode for the early stages of damage accumulation as it is the precursor of more severe damage modes, as will be shown in the subsequent sections [35].

16.3.2.1 Stiffness reduction model

Following the unifying formulation by [44] for shear lag models the effective longitudinal Young's modulus, $E_x^{(}$, can be calculated as a function of the crack spacing in the 90 degree layers as follows:

$$E_x^{(} = \frac{E_{x;0}}{1 + \alpha \frac{1}{2l} R} \quad [16.22]$$

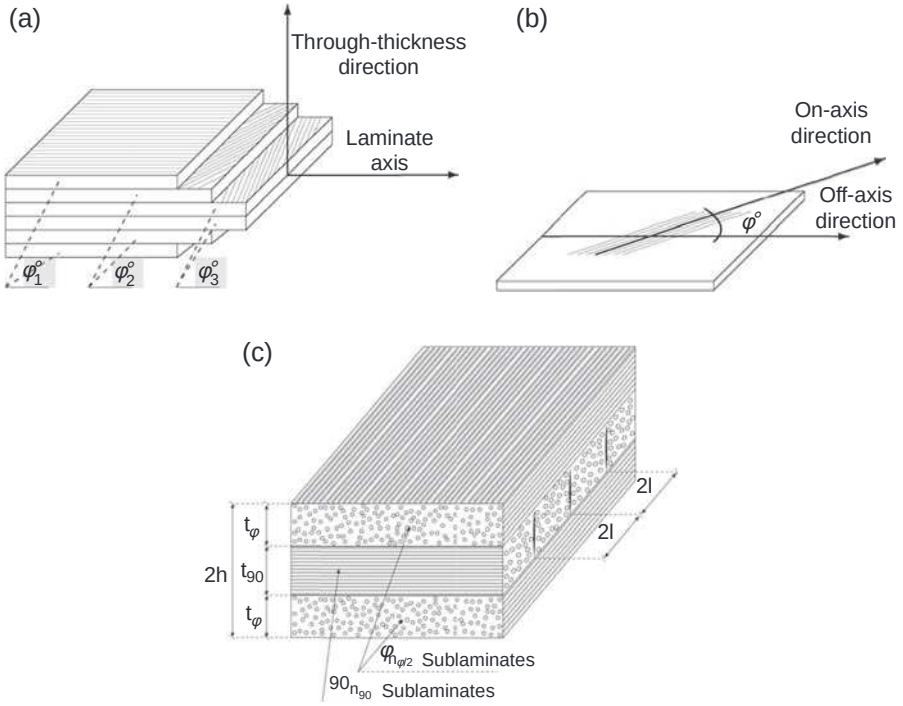

Figure 16.4 Panel (a): Schematic view of a fiber reinforced plastic (FRP) composite laminate of six plies and stacking sequence given by $[\varphi_1^\circ/\varphi_2^\circ/\varphi_3^\circ]_S$: Panel (b): Illustration of one of the plies with indication of material and laminate directions. Panel (c): Illustration for microscopic damage in $[\varphi_{\frac{n_f}{2}}/90_{n_{90}}/\varphi_{\frac{n_f}{2}}]$ laminate along with basic geometrical parameters.

where $E_{x,0}$ is the initial longitudinal Young's modulus of the undamaged laminate and $\bar{l} = \frac{l}{t_{90}}$ is the half crack-spacing normalized by the 90 degree sublaminate thickness, which can be expressed as a function of r as: $\bar{l} = \frac{1}{2r\,t_{90}}$. The function, $R(\bar{l})$, known as the average stress perturbation function, is defined as:

$$R(\bar{l}) = \frac{2}{\chi}\tanh(\chi\bar{l}) \qquad [16.23]$$

where χ is the shear lag parameter that can be obtained for the classical shear lag model [39,42] as follows:

$$\chi^2 = G_{23}\left(\frac{1}{E_2} + \frac{1}{l\,E_x^{(f)}}\right) \qquad [16.24]$$

The superscript (f) denotes "property of the $f_{\frac{n_f}{2}}$ -sublaminates" (see Fig. 16.4 for further details), and $l = t_f + t_{90}$. The term a in Eq. [16.22] is a function of the laminate mechanical and geometrical properties as follows:

$$a = \frac{E_2}{l E_1}\left(1 - n_{xy}^{(f)}\frac{\frac{n_{xy}^{(f)}}{E_y^{(f)}} + \frac{n_{12}}{E_2}}{\frac{1}{l E_y^{(f)}} + \frac{1}{E_1}}\right)\frac{1 - n_{12}n_{xy}^{(f)}}{1 - n_{12}^2\frac{E_2}{E_1}} \qquad [16.25]$$

For the sake of clearness the terms involved in Eqs. [16.22]e [16.25] are described in more detail in Table 16.1.

Table 16.1 Nomenclature of the terms used for shear lag analysis. Nominal values of ply and main geometry parameters are further provided in Table 16.4 in the context of a numerical example

Laminate		
	E_x	Longitudinal Young's modulus
	$E_x^{(}$	Effective long. Young's modulus
	h	Laminate half-thickness
Sublaminate		
	$E_x^{(f)}$	Longitudinal Young's modulus
	$E_y^{(f)}$	Transverse Young's modulus
	$n_{xy}^{(f)}$	In-plane Poisson ratio
	$G_{xy}^{(f)}$	In-plane shear modulus
	$G_{xz}^{(f)}$	Out-of-plane shear modulus
	t_{90}	$\frac{1}{2}(2n_{90})$+sublaminate half-thickness
	t_f	$f_{\frac{n_f}{2}}$ sublaminate thickness
	t	Ply thickness
Ply		
	E_1	Longitudinal Young's modulus
	E_1	Transverse Young's modulus
	n_{12}	In-plane Poisson ratio
	n_{23}	Out-of-plane Poisson ratio
	G_{12}	In-plane shear modulus
	G_{23}	Out-of-plane shear modulus

16.3.3 Selecting prognostics targets for fatigue in composites

Given a structure there are several structural elements and locations that can develop faults and are potential targets for prognostics. However, carrying out prognostics for all such elements can be prohibitive because of the computational cost. Therefore, a common approach is to prioritize more critical locations or identify "hot spots" that can be closely monitored. Additionally, prognostics rely on the capability of SHM to detect and localize fault location before predictions of fault growth can be made. Another key aspect to define is the damage magnitude threshold that must be used to define a structure's EOL, which is not necessarily the failure threshold. A suitable balance must be established in defining this threshold between using a very conservative threshold, at the expense of giving away useful remaining life; and a very aggressive threshold, resulting in potential structural failures. Such thresholds are typically defined over quantities that have a direct physical relation to failure criteria. A natural way to select a target for fatigue in composites would be by focusing on the reduction of effective strength during the life cycle, so that failure would occur when strength reduces below the maximum applied stress levels. However, given that strength cannot be measured nondestructively, other measurable properties such as degradation in materials Young's modulus are preferred for prognostics. Therefore, EOL for composite materials is proposed to be defined based on stiffness degradation criteria. Furthermore, it must be noted that establishing prognostics thresholds for fatigue degradation in composites is a complex task because damage progression heavily depends on factors like laminate stacking sequence, ply properties, and loading conditions. The choice of a suitable threshold generally depends on the application end use and the type of material used, and should be carefully examined when designing a prognostic system.

16.3.3.1 Competing damage modes

As mentioned in Section 16.3.2, it is generally accepted in the literature that matrix microcracking is the dominant fracture mode for the early stages of the fatigue process. Experimental observations [45] show that matrix microcracks density in off-axis plies asymptotically tends to an upper bounded value corresponding to a spacing of aspect ratio unity termed as characteristic damage state [3,46]. In addition to the characteristic damage state, damage progression may exceed other subcritical damage states before ultimate failure, corresponding, for instance, with the onset of local delaminations[2] [36] and fiber breakage [46,47]. These damage states define tolerance limits that can be chosen as damage thresholds for prognostics in composites. However, establishing a deterministic damage progression path to these subcritical states is not an easy task because of the uncertainty that arises in the growth and interactions of internal fracture modes from different scales. The aim of this section is not to address this question in depth but to provide a concise overview and discussion

[2] Local delaminations are small interlaminar fractures growing from the tips of matrix cracks.

Table 16.2 Selection of models for ERR due to local delamination induced by microcracks

Author	Classification	Energy release rate, G_{LD}
Takeda et al. [48]	One-dimensional (shear lag)	$\frac{t_{90}E_x^{\delta 90\rho}\delta_1 E_x^{\delta s\rho} + t_{90}E_x^{\delta 90\rho}\varepsilon_0^2}{2t_s E_x^{\delta s\rho}}\left(1 - \frac{4}{\delta\exp(\gamma\delta 1!\, d\rho) + \exp(-\gamma\delta 1!\, d\rho)}\right)^2$
Nairn and Hu [36]	Two-dimensional (variational)	$C_3 t_{90}\frac{E_x^{\delta 90\rho}}{E_x^{\delta l\rho}}Ds_x^2\frac{c^0\delta 0\rho! - c^0\delta 1! \, d\rho}{2}$

on this matter along with a summary of the methodology as used by the authors in Ref. [43]. Before going in details of the procedure a brief overview of main contributions addressing the interaction between damage modes is shown below.

16.3.3.2 Interaction of cracks and local delamination

This section addresses the case where a local delamination with length 2d has grown from the tips of matrix microcracks. It was shown in Ref. [48] that the effects of local delamination may vary depending on the stacking sequence used in a laminate. Here the discussion is focused on cross-ply laminates since it is widely used in the literature and also the numerical example presented later is based on this layup.

Table 16.2 highlights the main contributions to the formulation of term DG for the Eq. [16.19] under mixed-mode crack and delamination in cross-ply laminates.[3] The function c^0 as well as the terms C_1 and C_3 are given in the Appendix. The term x is given in the Eq. [16.24], and ε_0 represents the unitary axial deformation of the laminate subjected to the increase in applied tension $Ds_x = s_{x;max} - s_{x;min}$.

It is important to note that measuring local delamination by nondestructive evaluation techniques is still difficult, if not impossible, overall because local delaminations are dispersed widely in the laminate [45,49]. Therefore, a prognostics methodology that considers local delaminations needs further research in addition to requiring mature sensing technology capable of measurements of local delamination distributed over a large area in real time.

16.3.3.3 Global delamination

Global delamination is a damage mode consisting of interlaminar cracks arising between adjacent plies. The presence of global delaminations in composite structures typically carries other concomitant damage modes such as microcracks and local delamination [45,50]. For cross-ply laminates, global delamination may typically

[3] Certain formulations based on the COD approach by Gudmundson and Weilin [41] can also be considered to model the interaction between cracks and local-delamination [49]. Because of space limitation, they are not included here.

Table 16.3 Models of ERR for edge delamination. The terms $E_x^{(center)}$ and $E_x^{(edge)}$ are the effective stiffness measured at the center and edge of a laminate specimen, respectively. The rest of terms involved in these equations are grouped in Table 16.1

Author	Classification	Energy release rate G_{GD}
O'Brien et al. [54]	No interaction with cracks	$\frac{\varepsilon_0^2 h}{2}(E_{x,0} - E_x)$
Nairn [53]	Interaction with cracks	$\frac{1}{2}\left(\frac{\Delta s_x}{E_x}\right)\left(E_x^{(center)} - E_x^{(edge)}\right)$

be expected at the final stage of the fatigue damage process, coinciding when local delaminations induce a damage so severe that the catastrophic failure can occur at any time (even before the onset of global delamination) [48]. On the other hand, matrix microcracks might induce global delamination areas in quasiisotropic and angle-ply laminates so that they are located at the free-edges of the laminate, and they can appear at earlier stages of the fatigue process [45,50]. Thus, in the latter cases, delamination onset and growth should be predicted in parallel to matrix microcracks.

To account for the global delamination within the formulation of ERR, different models are available in the literature. Table 16.3 gives an overview of two of the most referred models for the ERR accounting for global delamination. The reader is also referred to the work of Hosoi et al. [51,52] for a detailed study about the interaction between microcracks and edge delamination based on the energy model of Nairn et al. [53].

16.3.3.4 Balance of energies

Based on a balance of energies between different plausible damage modes (namely, transverse cracks, local delamination, and global delamination), one can address the question of whether the next increment in fatigue damage will be through another transverse crack or a different damage mode induced by the existing microcracks [36]. See Fig. 16.5, where the concept of balance of energies between plausible damage modes is illustrated through a case study for a $[0_2/90_4]_S$ cross-ply laminate taken from the composites data set from NASA Ames Prognostics Data Repository [55].

In Fig. 16.5 the terms TC, LD, and GD refer to transverse cracks, local delamination, and global delamination, respectively. Among the possibilities presented in Tables 16.2 and 16.3 the models by Nairn and Hu [36] and T.K. O'Brien et al. [54] have been chosen to obtain the LD and GD curves. The square markers are to denote the points where a change in the dominant fracture mode is expected. Observe that initially the release of energy for transverse cracks is larger than that of the rest of damage modes, then matrix microcracks are expected to accumulate at a faster rate at earlier cycles. Observe also that the point where TC and LD curves intersect defines a critical value for the matrix microcracks density, because from this point, local

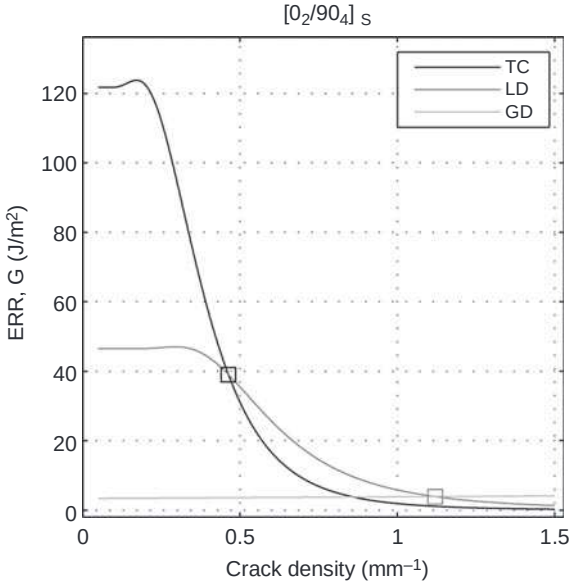

Figure 16.5 ERR term as a function of the matrix crack density for different damage modes. The square markers delimit the points where a change in the dominant fracture mode is expected.
Figure extracted from Chiachío J, et al. An energy-based prognostics framework to predict fatigue damage evolution in composites. In: Annual conference of the prognostics and health management society. New Orleans LA: Prognostics and Health Management Society; 2013.

delaminations are more likely to appear than another matrix microcrack hence defining saturation stage for microcracks. Results also show that until the final stage of the process the local delamination mode releases more strain energy than the global delamination mode. Therefore, global delamination onset is expected at the very late stage of the fatigue damage process. These conclusions agree well with the experimental evidence obtained for cross-ply laminates reported in Jamison [45] and also with the data set from Saxena et al. [55].

Based on this reasoning, prognostics thresholds can be established by predicting the position of these reference points as the fatigue process continues. Notice that the energy term DG depends on model parameters which are sequentially updated as new data arrives, as will be shown in the next section. Hence, the intersection points defining the thresholds dynamically shift their position until a convergence stage, as was reported in Chiachío et al. [43].

For this work the progression of damage is studied by focusing on the matrix microcracks density and the stiffness loss induced by the microcracking. In both cases, non-destructive evaluation (NDE) measurements are possible using today's sensing technology. The saturation stage of microcracks along with a limiting value for stiffness loss are selected as microscale and macroscale damage thresholds, respectively. Microscale damage thresholds based on more severe damage modes

(local delamination and global delamination) would also be possible provided that online measurements can be obtained, however, it is at the expense of greater uncertainty because of the complex interactions between damage modes.

16.3.4 Model-based damage prognostics in composites

Having defined the model for damage propagation forward in time, the next step is to develop a method for sequentially estimating the damage state as long as new SHM data are collected. As a previous step a probability-based description of the deterministic models described in Section 16.3.2 is first required.

As discussed in Section 16.3.2 the progression of damage is studied at every cycle n by focusing on the matrix microcrack's density, r_n, and the normalized effective stiffness defined as $D_n = \frac{E'_x}{E_{x;0}}$, so that the following joint state transition equation of two components $g = [g_1, g_2]$ can be defined as follows:

$$x_{1_n} = r_n = g_1(r_{n-1}; q) + v_{1_n} \quad \text{Eq: 16:21} \qquad [16.26]$$

$$x_{2_n} = D_n = g_2(r_n; q) + v_{2_n} \quad \text{Eq: 16:22} \qquad [16.27]$$

In the last equation, subscripts 1 and 2 denote the corresponding damage subsystems: matrix microcrack density and relative stiffness reduction, respectively. Observe that the three main elements defining a stochastic damage statee space model can be identified in Eqs. [16.26] and [16.27]: (1) the system output $x_n = [r_n, D_n] \in R^2$, (2) the forward model of damage evolution $g = [g_1, g_2]$, and (3) the corresponding model error vector $v_n = [v_{1_n}; v_{2_n}] \in R^2$. It is important to remark that the model errors v_{1_n} and v_{2_n} are stochastically independent even though the models corresponding to the damage subsystems, namely g_1 and g_2, are mathematically related, as shown in Section 16.3.2. This means that the covariance operator S_{v_n} is a diagonal matrix, ie, $S_{v_n} = \mathrm{diag}(s^2_{v_{1;n}}; s^2_{v_{2;n}})$, where $s_{v_{1;n}}$ and $s_{v_{2;n}}$ are the corresponding standard deviations of the errors v_{1_n} and v_{2_n}, respectively. Therefore, the stochastic damage model of the overall system can be readily expressed as a product of univariate Gaussians, as:

$$p(x_n | x_{n-1}; q) = p(D_n | r_n; q)\, p(r_n | r_{n-1}; q) \qquad [16.28]$$

where

$$p(r_n | r_{n-1}; q) = \frac{1}{\sqrt{2\pi}\, s_{v_{1;n}}} \exp\left(-\frac{(r_n - g_1(r_{n-1}; q))^2}{2 s^2_{v_{1;n}}}\right) \qquad [16.29]$$

$$p(D_n|r_n;q) = \frac{1}{\sqrt{2\pi}\,s_{v_{2;n}}} \exp\left(-\frac{(D_n - g_2(r_n;q))^2}{2s_{v_{2;n}}^2}\right) \quad [16.30]$$

Next, let $y_n = [y_{1_n}; y_{2_n}] = [h_{1_n}; D_n] \in R^2$ be the measurements to the system response, thus the following measurement equation, as that defined in Eq. [16.2], is added to the discrete statee space model to account for the measurement error term $w_n \in R^2$:

$$p(y_n|x_n;q_n) = \frac{1}{(2\pi)^{\frac{2}{2}}|S_{w_n}|^{\frac{1}{2}}} \exp\left(-\frac{1}{2}(y_n - x_n)^T \sum_{w_n}^{-1} (y_n - x_n)\right) \quad [16.31]$$

The measurements of each subsystem (microcracks density and relative stiffness decrease) are considered as stochastically independent, thus $S_{w_n} = \mathrm{diag}(s_{w_{1;n}}^2; s_{w_{2;n}}^2)$, where $s_{w_{1;n}}$ and $s_{w_{2;n}}$ are the standard deviations of the corresponding measurement errors w_{1_n} and w_{2_n}, respectively. Finally, the measurement equation can be readily defined as:

$$p(y_n|x_n;q_n) = p(b_n|r_n)\, p(D_n|D_n) \quad [16.32]$$

where

$$p(b_n|r_n) = \frac{1}{\sqrt{2\pi}\,s_{w_{1;n}}} \exp\left(-\frac{(b_n - r_n)^2}{2s_{w_{1;n}}^2}\right) \quad [16.33]$$

$$p(D_n|D_n) = \frac{1}{\sqrt{2\pi}\,s_{w_{2;n}}} \exp\left(-\frac{(D_n - D_n)^2}{2s_{w_{2;n}}^2}\right) \quad [16.34]$$

The PDF of the initial damage state x_0 together with the PDFs for the state transition equation and the measurement equation as stated in Eqs. [16.28] and [16.32], provide a complete statistical description of the overall system and play a major role in the filtering-based prognostics methodology explained above.

In the last equations the model parameters, q, are selected among the complete set of mechanical and geometrical parameters describing Eqs. [16.19]e [16.24] through a global sensitivity analysis based on variances following the methodology proposed by Saltelli et al. [56]. The ply properties {E_1, E_2, t} along with the Paris' law fitting parameter a emerged as sensitive parameters to the model output uncertainty [57], so they are selected for sequential updating as shown below. Furthermore, the standard deviations of the model errors v_{1_n} and v_{2_n} are added as candidates for updating since

they are uncertain a priori, thereby resulting in the model parameter vector, $q = [a; E_1; E_2; t; s_{v_{1:n}}; s_{v_{2:n}}] \in R^6$. The probabilistic information of parameters is specified in the next section.

16.4 Prognostics example

In this section the prognostic framework discussed above is applied to fatigue load testing data from a run-to-failure experiment in cross-ply $[0_2/90_4]_S$ graphitee epoxy laminates. The tests were conducted under load-controlled tensione tension cyclic loading with a maximum applied load of 31.13 kN, a frequency $f = 5$ Hz, and a stress ratio $R = 0.14$ (relation between the minimum and maximum stress for each cycle) [55,57,58]. A set of 12 piezoelectric discs (or piezoelectric PZT-material sensors) was used to monitor the effects of matrix microcracks density and delamination, along with a set of triaxial strain gauges to measure the normalized effective stiffness. Additionally, periodic X-ray images were taken to assess internal damage and this information was used to map the effects observed in sensor data to actual damage. The mapping between PZT raw data and microcrack density from X-ray images was carried out by manually observing and quantifying the damage and using signal processing to extract damage relevant features from PZT data. Detailed methodology can be found in Larrosa and Chang [59]. Damage data used in this example correspond to laminate L1S19 from the fatigue data set [55] (the reader is referred to Table A.1 from Refs [57,60] for further insight).

Algorithm 2: Systematic importance resampling (SIR) particle filter.

1. At $n = 0$ h$
2. Initialize $x_0^{(1)}; q_0^{(1)}; \ldots; x_0^{(i)}; q_0^{(i)}; \ldots; x_0^{(N)}; q_0^{(N)}$, where $x_0^{(i)}; q_0^{(i)} \sim p(q)p(x_0|q)$
3. Assign the initial weights: $\{u_0^{(i)} = 1/N\}_{i=1}^{N}$
4. At $n > 1$ f time n evolves as new data point arrivesg
5. for $i = 1 : N$ do
6. Sample from Eq. [16.8]: $q_n^{(i)} \sim p(q_n|q_{n-1}^{(i)})$ (eg, use the method by Daigle [29])
7. Sample from Eq. [16.29]: $r_n^{(i)} \sim p(r_n|r_{n-1}^{(i)}; q_n^{(i)})$
8. Sample from Eq. [16.30]: $D_n^{(i)} \sim p(D_n|D_{n-1}^{(i)}; q_n^{(i)})$
9. Set $z_n^{(i)} = \{r_n^{(i)}; D_n^{(i)}; q_n^{(i)}\}$ and $z_{0:n}^{(i)} = \{z_{0:n-1}^{(i)}; z_n^{(i)}\}$
10. Update weights: $w_n^{(i)} \propto w_{n-1}^{(i)} p(z_n|z_n^{(i)}) p(z_n^{(i)}|z_{n-1}^{(i)}) u_{n-1}^{(i)}$
11. end for
12. for $i = 1 : N$ do
13. Normalize $u_n^{(i)}$) $w_n^{(i)} = w_n^{(i)} / \sum_{i=1}^{N} w_n^{(i)}$
14. end for
15. $\{x_n^{(i)}; q_n^{(i)}\}_{i=1}^{N}$) Resample $\{x_n^{(i)}; q_n^{(i)}; u_n^{(i)}\}_{i=1}^{N}$

Results for sequential state estimation along with multistep ahead prediction for both microcrack density and normalized effective stiffness are shown at three different time (cycle) positions in Fig. 16.6. Microcrack density is expressed in cracks per mm and normalized effective stiffness is dimensionless. Note that at the beginning of each plot (left side before the multistep ahead prediction of states) the collected data up to cycle $n = \{1,4,8\} \times 10^4$ are plotted along with the sequence of filtered states, which are obtained using Algorithm 2 with $N = 5000$ particles. For this example, the SIR

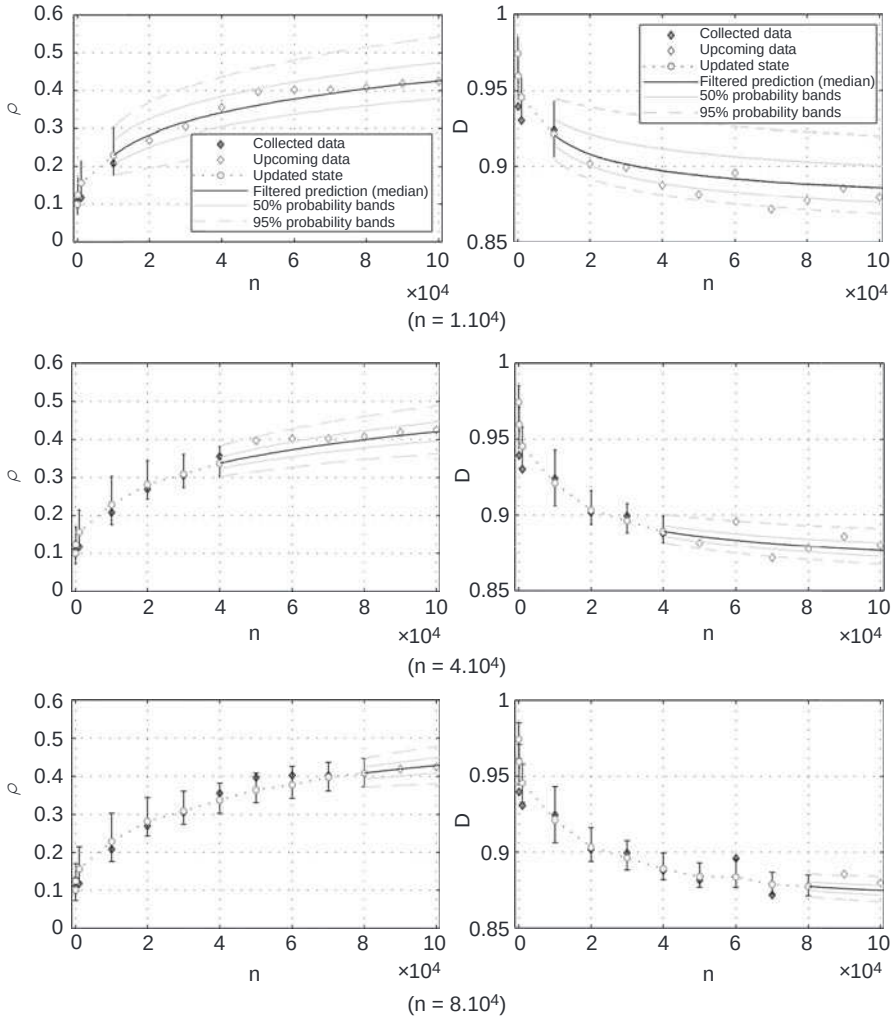

Figure 16.6 Sequential state estimation for matrix microcracks density (right panels), and normalized effective stiffness (left panels) up to a certain cycle n, where $n = 1 \times 10^4$, 4×10^4, and 8×10^4. The multistep ahead predicted damage states are represented using dashed gray lines for the 5! 95% probability bands and solid gray lines for the 25! 75% probability bands.

version of the SIS algorithm is adopted. Initial values for the damage states are $x_0 = (r_0, D_0)$, where $r_0 = 0.1$ cracks/mm and $D_0 = 1$ (dimensionless). The standard deviation of the measurement error parameters are set to $s_{w1,n} = 0.05$ cracks mm and $s_{w2,n} = 0.01$. Chosen prior PDFs for model parameters $q = \{q_1, q_2, \ldots, q_6\}$ are specified in Table 16.4. The diagonal elements of the covariance matrix $S_{x_{0j}}$ (recall Eq. [16.8]) are appropriately selected through initial test runs and set to 0.5% of the 5e 95th band of the prior PDFs for the jth component of q.

Updated damage states are further forward propagated into the future to compute the EOL and RUL following the methodology described in Section 16.2.3.4. The useful domain is defined here as $U = \{r, D : 0 \le r \le 0.418 \text{ \& } 0 \le D \le 0.875\} \subset R^2$.

The results of RUL estimates together with their quantified uncertainty by the 25! 75% probability bands are plotted against time in Fig. 16.7, where two cones of accuracy at 10% and 20% of true RUL, denoted as RUL*, are drawn to help evaluate the prediction accuracy and precision. Observe that the RUL prediction is appreciably inaccurate within the first stage of the fatigue process, that corresponds to the initial parameter tuning period, ie, length of time required for SHM data to train the model parameters. Moving forward beyond this period the prediction performance noticeably improves with increasing cycles. As fatigue cycles evolve, not only the prediction means improve (values closer to RUL* line) but also the prediction spread gets narrower. This visualization allows assessment of how prediction performance

Table 16.4 Nominal values and prior uncertainty of model parameters used in calculations. The rest of parameters in damage mechanics models (Eqs. [16.22] and [16.23]) can be obtained using the classical laminate plate theory [61e 63]. The nominal values for fitting parameters have been defined through initial fitting tests

Type	Parameter	Nominal value	Units	COV(%)	Prior PDF
Mechanical	E_1	127.55	GPa	10	Log N
	E_2	8.41	GPa	10	Log N
	G_{12}	6.20	GPa	d	Not applicable
	n_{12}	0.31	d	d	Not applicable
	G_{23}	2.82	GPa	d	Not applicable
	t	1.5 & 10^{-4}	m	10	Log N
Fitting	a	1.8	d	20	Log N
	A	10^{-4}	d	d	Not applicable
Error	s_{v1}	d	#Cracks/ (m & cycle)	d	U(0.5,1.5)
	s_{v2}	d	d	d	U(0.001,0.003)

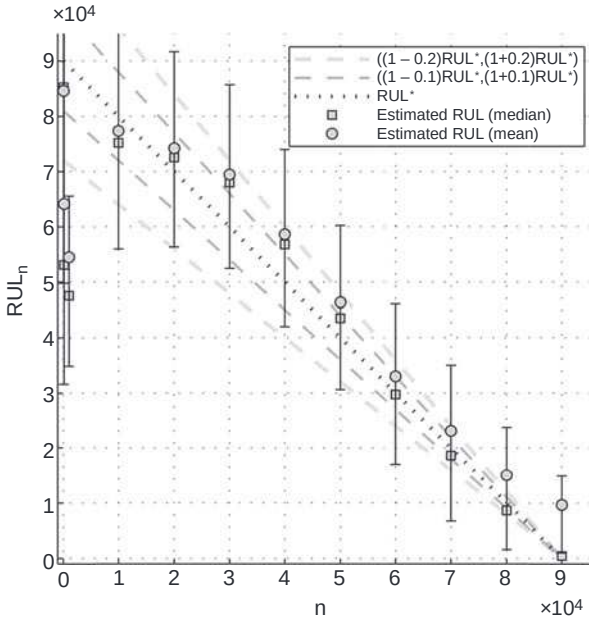

Figure 16.7 RUL versus fatigue cycles plot to assess lifetime prediction performance for composites under fatigue aging. Two cones of accuracy at 10% and 20% of true RUL are represented to help evaluating prognostics performance. Darker dashed lines represent the cone of accuracy at 10%. The true RUL, denoted as RUL*, is represented using black dotted line.

changes over time in terms of correctness (accuracy and precision). Also, by means of the prognostics horizon (PH), it is possible to assess how quickly performance converges within desired accuracy levels. In this example the PH for 0.2 as a-accuracy is PH ¼ 8$10^4$! 1$10^3$ ¼ 7.9$10^4$ cycles. Observe also that from cycle n ¼ 5$10^4$ the estimated mean values for the RUL (labeled by the circles in Fig. 16.7) move away from the RUL* line and they progressively leave the accuracy cone as fatigue cycles evolve. However, the median RUL estimates (labeled by the squares) remain within the accuracy region during all the process. An explanation for this observation is provided in view of the asymptotic behavior of the damage process for both, microcrack density and normalized stiffness decrease (see Fig. 16.6). Indeed, from cycle n ¼ 5$10^4$, the model produces a large amount of predicted samples that already lie within the failure domain $\overline{U}$ at the instant of prediction n. This leads to an increasing higher density of predicted RUL_n outcomes concentrated at cycle n as well as a distribution tail of RUL_n corresponding to cycles higher than n. As a consequence the mean predicted RUL values have a positive shift with respect to the RUL* values because of such a distribution tail, whereas the median RUL estimates remain closer to the RUL* line.

It must be noted that observations like these are situation specific and this example only illustrates how prognostic results must be interpreted especially considering

uncertainty in the predictions. A brief discussion about interpreting such behaviors can be found in Saxena et al. [21] and may be related to the difficulty of obtaining adequate amount of measurements to account for behaviors when the damage process has reached asymptotic growth behavior.

16.5 Concluding remarks

Prognostic information about a component fault/damage can be a valuable resource in determining an appropriate course of action to avoid failures. Potential of prognostics in positively contributing to safety and improving life cycle costs is equally relevant to existing legacy systems and new system designs. Legacy systems adopt additional sensing and processing with a potentially high price of retrofitting and additional validation and/or certification costs to gain extended system life and safety factor. New system designs can significantly reduce these costs if prognostics and health management are adopted early in the design to facilitate a more optimal sensor placement for observability and coverage. This, however, requires integration of health management design into the systems engineering process. Depending on the system design and how SHM is integrated into that design, there are several approaches that can be taken to implement a prognostic system. This chapter presented a novel model-based prognostics framework to make predictions of EOL and RUL of composites under fatigue conditions and estimate the uncertainty associated with these predictions. This is done by fusing the experimental information and models available at different levels of granularity by means of the Bayes' theorem and total probability theorem. The validity of this framework was demonstrated on SHM data collected from a tensione tension fatigue experiment using a carbon fiber reinforced plastic cross-ply laminate. The results have demonstrated that anticipating the EOL of composites subjected to fatigue conditions is possible provided that measurements of damage can be sequentially collected.

References

[1] Vasiliev VV, Morozov EV. Mechanics and analysis of composite materials. 2001.
[2] Degrieck J, Paepegem WV. Fatigue damage modeling of fibre-reinforced composite materials: review. Appl Mech Rev 2001;54(4).
[3] Reifsnider KL, Talug A. Analysis of fatigue damage in composite laminates. Int J Fatigue 1980;2(1):3e 11.
[4] Jamison RD, et al. Characterization and analysis of damage mechanisms in tension-tension fatigue of graphite/epoxy laminates. In: Effects of defects in composite materials. ASTM; 1984. p. 21e 55.
[5] Myötyri E, Pulkkinen U, Simola K. Application of stochastic filtering for lifetime prediction. Reliab Eng Syst Saf 2006;91(2):200e 8.
[6] Cadini F, Zio E, Avram D. Monte Carlo-based filtering for fatigue crack growth estimation. Probab Eng Mech 2009;24(3):367e 73.

[7] Zio E, Maio FD. Fatigue crack growth estimation by relevance vector machine. Expert Syst Appl 2012;39(12):10681e 92.
[8] An D, Choi J-H, Kim NH. Prognostics 101: a tutorial for particle filter-based prognostics algorithm using matlab. Reliab Eng Syst Saf 2013;115:161e 9.
[9] Gobbato M, Kosmatka JB, Conte JP. A recursive Bayesian approach for fatigue damage prognosis: an experimental validation at the reliability component level. Mech Syst Signal Process 2014;45(2):448e 67.
[10] Boller C, Buderath M. Fatigue in aerostructuresd where structural health monitoring can contribute to a complex subject. Philos Trans R Soc A 2007;365:561e 87.
[11] Farrar CR, Lieven NAJ. Damage prognosis: the future of structural health monitoring. Philos Trans R Soc A Math Phys Eng Sci 2007;365(1851):623e 32.
[12] Gobbato M, et al. A reliability-based framework for fatigue damage prognosis of composite aircraft structures. Probab Eng Mech 2012;29:176e 88.
[13] Henley S, Hess A, Fila L. The joint strike fighter (JSF) PHM and the autonomic logistic concept: potential impact on aging aircraft problems. In: The RTO applied vehicle technology panel (AVT) Specialists' meeting; 2001 [Manchester, UK].
[14] McColl J. Hums in the era of CAA, JAA, EASA and ICAO. In: AIAC Conference; 2005 [Melbourne].
[15] Silverman H. T-HUMS-AH64 lead the fleet (LTF) summary and glimpse at hermes 450 MT- HUMS. In: AIAC conference; 2005 [Melbourne].
[16] NASA. PHM design process. NASA: Prognostics Center of Excellence; 2012.
[17] Rajamani R, et al. Developing IVHM requirements for aerospace systems. In: SAE AeroTech congress and exhibition. Montreal, Canada: SAE; 2013.
[18] Sikorska JZ, Hodkiewicz M, Ma L. Prognostic modelling options for remaining useful life estimation by industry. Reliab Eng Syst Saf 2011;25:1803e 36.
[19] Papadimitriou C, Beck JL, Au SK. Entropy-based optimal sensor location for structural model updating. J Vib Control 2000;6(12):89e 110.
[20] Saxena A, et al. Requirement flowdown for prognostics health management. In: AIAA Infotech@Aerospace; 2012 [Garden Grove, CA].
[21] Saxena A, et al. Metrics for offline evaluation of prognostic performance. Int J Prognostics Health Manag 2010;1(1):20.
[22] Saxena A, et al. Metrics for evaluating performance of prognostic techniques. In: IEEE international conference on prognostics and health management; 2008 [Denver, CO].
[23] Saxena A, Shankararaman S, Goebel K. Performance evaluation for fleet-based and unit-based prognostic methods. In: European Conference of the Prognostics and Health Management Society; 2014 [Nantes, France].
[24] Jaynes ET. Probability theory: the logic of science. Cambridge University Press; 2003.
[25] Gordon NJ, Salmond DJ, Smith AFM. Novel approach to nonlinear/non-Gaussian Bayesian state estimation. IEEE-Proceedings-F 1993;140:107e 13.
[26] Liu J, West M. Combined parameter and state estimation in simulation-based filtering. In: Doucet A, Freitas N, Gordon N, editors. Sequential Monte Carlo methods in practice, statistics for engineering and information science. New York: Springer; 2001.
[27] Kantas N, et al. An overview of sequential Monte Carlo methods for parameter estimation in general state-space models. In: 15th IFAC symposium on system identification; 2009.
[28] Storvik G. Particle filters for state-space models with the presence of unknown static parameters. IEEE Trans Signal Process 2002;50(2):281e 9.
[29] Daigle M, Goebel K. Model-based prognostics with concurrent damage progression processes. IEEE Trans Syst Man, Cybern Syst 2013;43(3):535e 46.

[30] Arulampalam MS, et al. A tutorial on particle filters for online nonlinear/non-Gaussian Bayesian tracking. IEEE Trans Signal Process 2002;50(2):174e 88.
[31] Doucet A, Freitas ND, Gordon N. An introduction to sequential Monte Carlo methods. In: Doucet A, Freitas ND, Gordon N, editors. Sequential Monte Carlo methods in practice. New York: Springer; 2001. p. 3e 14.
[32] Doucet A, Freitas ND, Gordon N. Sequential Monte Carlo methods in practice. New York: Springer Verlag; 2001.
[33] Bogdanoff JL, Kozin F. Probabilistic models of comulative damage. John Wiley & Sons; 1985.
[34] Paris PF, Gomez MP, Anderson W. A rational analytic theory of fatigue. Trend Eng 1961; 13:9e 14.
[35] Abrate S. Matrix cracking in laminated composites: a review. Compos Eng 1991;1(6): 337e 53.
[36] Nairn JA, Hu S. The initiation and growth of delaminations induced by matrix microcracks in laminated composites. Int J Fract 1992;57(1):1e 24.
[37] Nairn JA. The strain energy release rate of composite microcracking: a variational approach. J Compos Mater 1989;23(11):1106e 29.
[38] Talreja R, Singh CV. Damage and failure of composite materials. Cambridge University Press; 2012.
[39] Garrett K, Bailey J. Multiple transverse fracture in 90 cross-ply laminates of a glass fibre-reinforced polyester. J Mater Sci 1977;12(1):157e 68.
[40] Hashin Z. Analysis of cracked laminates: a variational approach. Mech Mater 1985;4(2): 121e 36.
[41] Gudmundson P, Weilin Z. An analytic model for thermoelastic properties of composite laminates containing transverse matrix cracks. Int J Solids Struct 1993;30(23): 3211e 31.
[42] Manders PW, et al. Statistical analysis of multiple fracture in 0/90/0 glass fibre/epoxy resin laminates. J Mater Sci 1983;18(10):2876e 89.
[43] Chiachío J, et al. An energy-based prognostics framework to predict fatigue damage evolution in composites. In: Annual conference of the prognostics and health management society. New Orleans LA: Prognostics and Health Management Society; 2013.
[44] Joffe R, Varna J. Analytical modeling of stiffness reduction in symmetric and balanced laminates due to cracks in 90 layers. Compos Sci Technol 1999;59(11):1641e 52.
[45] Jamison RD. The role of microdamage in tensile failure of graphite/epoxy laminates. Compos Sci Technol 1985;24(2):83e 99.
[46] Beaumont PWR, Dimant RA, Shercliff HR. Failure processes in composite materials: getting physical. J Mater Sci 2006;41(20):6526e 46.
[47] Lee JW, Allen DH, Harris CE. Internal state variable approach for predicting stiffness reductions in fibrous laminated composites with matrix cracks. J Compos Mater 1989; 23(12):1273e 91.
[48] Takeda N, Ogihara S. Initiation and growth of delamination from the tips of transverse cracks in CFRP cross-ply laminates. Compos Sci Technol 1994;52(3):309e 18.
[49] Schmutzler H, et al. Degradation monitoring of impact damaged carbon fibre reinforced polymers under fatigue loading with pulse phase thermography. Compos Part B Eng 2014;59:221e 9.
[50] Nairn JA. Matrix microcracking in composites. In: Talreja R, Manson JAE, editors. Polymer matrix composites. Amsterdam: Elsevier Science; 2000. p. 403e 32.

[51] Hosoi A, et al. High-cycle fatigue characteristics of quasi-isotropic CFRP laminates over 108 cycles (initiation and propagation of delamination considering interaction with transverse cracks). Int J Fatigue 2010;32(1):29e 36.
[52] Hosoi A, et al. Quantitative evaluation of fatigue damage growth in CFRP laminates that changes due to applied stress level. Int J Fatigue 2011;33(6):781e 7.
[53] Nairn JA. Fracture mechanics of composites with residual thermal stresses. J Appl Mech 1997;64:804e 15.
[54] O'Brien TK, Rigamonti M, Zanotti C. Tension fatigue analysis and life prediction for composite laminates. Int J fatigue 1989;11(6):379e 93.
[55] Saxena A, et al. CFRP composites dataset. 2013.
[56] Saltelli A, et al. Global sensitivity analysis: the primer. Wiley-Interscience; 2008.
[57] Chiachío J, et al. Bayesian model class selection and parameter estimation for fatigue damage progression in composites. Int J Fatigue 2015;70:361e 73.
[58] Saxena A, et al. Accelerated aging experiments for prognostics of damage growth in composites materials. In: International workshop on structural health monitoring; 2011.
[59] Larrosa C, Chang F-K. Real time in-situ damage classification, quantification and diagnosis for composite structures. In: 19th international congress on sound and vibration; 2012.
[60] Chiachío M, et al. An efficient simulation framework for prognostics of asymptotic processes- a case study in composite materials. In: European Conference of the Prognostics and Health Management Society. Nantes, France: PHM Society; 2014.
[61] Tsai SW. Theory of composites design. Think Composites; 1992.
[62] Tsai SW. Strength and life of composites. USA: Stanford University; 2008.
[63] Tsai SW, Wu EM. A general theory of strength for anisotropic materials. J Compos Mater 1971;5(1):58.

Appendix: Nomenclature and basic relations

Expressions for $c(l)$ and its first derivate $c'(l)$ are given by:

$$c(l) = 2a_1a_2\left(a_1^2+a_2^2\right)\frac{\cosh(a_1l)\cos(a_2l)}{a_2\sinh(a_1l)\sin(a_2l)}$$

$$c'(l) = 4a_1a_2\left(a_1^2+a_2^2\right)\frac{\sinh(a_1l)\sin(a_2l)}{a_2\sinh(a_1l)\sin(a_2l)+a_1\sin(a_2l)} \quad [16.35]$$

$$c(l) = a_1a_2\left(a_1^2-a_2^2\right)\frac{\tanh(a_2l)\tanh(a_1l)}{a_2\tanh(a_2l)-a_1\tanh(a_1l)}$$

$$c'(l) = a_1^2a_2^2\left(a_1^2-a_2^2\right)^2\frac{\frac{\tanh(a_2l)}{\cosh^2(a_1l)}-\frac{\tanh(a_1l)}{\cosh^2(a_2l)}}{a_2\tanh(a_2l)-a_1\tanh(a_1l)} \quad [16.36]$$

where $a_1 = -\frac{p}{2} + \sqrt{\frac{p^2}{4} - q}$ and $a_2 = -\frac{p}{2} - \sqrt{\frac{p^2}{4} - q}$. The Eq. [16.35] applies when $\frac{4q}{p^2} > 1$. Otherwise, Eq. [16.36] should be considered. The terms p and q are relations of the ply properties and the stacking sequence defined by $p = (C_2 - C_4)C_3$, $q = C_1C_3$. The parameters C_i, i:1,. ,4, are known functions of the laminate properties defined as:

$$C_1 = \frac{1}{E_1} + \frac{1}{\lambda E_2} \quad [16.37]$$

$$C_2 = \lambda + \frac{2}{3}\left(\frac{n_{23}}{E_2} - \frac{\lambda n_{12}}{3E_1}\right) \quad [16.38]$$

$$C_3 = \delta(1 + \lambda) + 3\lambda^2 + 12\lambda + 8\left[\frac{1}{60E_2}\right] \quad [16.39]$$

$$C_4 = \frac{1}{3}\left(\frac{1}{G_{23}} + \frac{\lambda}{G_{12}}\right) \quad [16.40]$$

where λ is the ply-thickness ratio $\lambda = t_0/t_{90}$. Notice that DG_{LD} depends on the magnitude $\delta(\bar{\lambda} - d\bar{P})$, which expresses the separation between the tips of two growing delaminations starting from the tips of the matrix microcracks. With no loss of generality, thermal stresses are not considered for the formulation of ERR in Tables 16.2 and 16.3, as the data used for this work, and also in most of the fatigue experiments, are collected in a temperature-controlled environment.

This page intentionally left blank

This page intentionally left blank

Over the last twenty years the area of Structural Health Monitoring (SHM) has experienced spectacular progress. The widespread adoption of SHM could both significantly improve safety and reduce maintenance and repair expenses, estimated to be about a quarter of an aircraft fleet's operating costs. The SHM field encompasses trans-disciplinary areas including smart materials, sensors and actuators, damage diagnosis and prognosis, signal and image processing algorithms, wireless intelligent sensing, data fusion and energy harvesting. This book focuses on how SHM techniques are applied to aircraft structures with particular emphasis on composite materials.

The book is divided into four main parts. The first part provides an overview of SHM technologies for damage detection, diagnosis and prognosis in aerospace structures. Part Two moves on to analyse smart materials for SHM in aerospace structures, such as piezoelectric materials, optical fibers and flexoelectricity. This part also includes two vibration-based energy harvesting techniques for powering wireless sensors based on piezoelectric electromechanical coupling and diamagnetic levitation concepts. Part Three explores innovative SHM technologies for damage diagnosis in aerospace structures. Chapters within this section include sparse array and phase array techniques for damage detection. The final section of the volume details innovative SHM technologies for damage prognosis in aerospace structures.

Structural Health Monitoring (SHM) in Aerospace Structures will be a key reference for researchers working within this industry, academic and government research agencies developing new systems for the SHM of aerospace structures and materials scientists.

Prof. Fuh-Gwo Yuan is Samuel P. Langley Distinguished Professor in the Mechanical and Aerospace Engineering Department of North Carolina State University, Raleigh, and National Institute of Aerospace, Hampton, Virginia, USA.

ISBN 978-0-08-100148-6

9 780081 001486

WP
WOODHEAD PUBLISHING
An imprint of Elsevier • elsevier.com

ELSEVIER